Characterizing the Structure of Lithium Metal Batteries using Local Ultrasonic Resonance Spectroscopy (LURS)

Matthew Webster*, Daniel Perey, Yi Lin, and Erik Frankforter
NASA Langley Research Center, 3 E. Taylor St., Hampton, VA, USA 23681

ABSTRACT

Nondestructive characterization of battery structures is important as both a research tool and as a means for developing reliable prognostics for batteries in service. Local ultrasonic resonance spectroscopy (LURS) is a technique that measures spatially localized through-thickness vibrational resonances in layered materials. In battery cells, LURS measurements can reveal layer spacing and changes in mechanical properties. This study examines changes in structure that occur from fabrication to end of life for batteries cycled under different conditions as a demonstration of the capabilities of the LURS approach.

Lithium metal pouch cell batteries were studied in both single- and multi-layer form factors. The cells were electrically cycled under constant current conditions at charge rates ranging from 0.2 C to 2 C, where 1 C is the charge rate (C-rate) required to fully charge a battery in one hour. In addition to varying charge rates, cells were also cycled under different temperatures and loading conditions, leading to a wide variety of electrode structures at end of life.

LURS scans were conducted at various points in the battery lifetime to examine how damage developed. Multiple processing methods are shown, which help to reveal information about the internal resonance in each case and the ways in which resonance changes due to cell aging and spatial variation in the layered structure. Scan data in some instances showed evidence of manufacturing defects such as foreign object debris (FOD) on the electrode surface. In other cases, scan data showed spatial variation in degradation of the lithium anode surface that was dependent on the charge rate, loading scenario, or cycling temperature.

Keywords: Ultrasound, lithium metal batteries, nondestructive evaluation, resonance

1. INTRODUCTION

The electrochemical performance and safety of lithium-based batteries are both closely tied to their internal structure. This includes both the as-manufactured structure and the ways that the structure changes during electrochemical cycling. Electrode defects from manufacturing impact cell efficiency, capacity, and the rate of capacity loss during cycling [1], while foreign object debris (FOD) could potentially lead to short circuit and prevent the cells from cycling at all. In viable lithium-metal cells, the internal structure changes as lithium is stripped and re-plated during electrochemical cycling. In some instances, irregular plating of lithium can form dendrites that could potentially penetrate the separator between the anode and cathode and cause catastrophic failure. Even in less catastrophic cases, irregular plating can affect the electrochemical performance through "dead lithium" buildup on the bulk anode surface, decreasing the cell capacity over time [2]. A means of performing nondestructive evaluation (NDE) of the internal structure of batteries is needed for manufacturing quality control and as a means of studying degradation mechanisms associated with cell aging.

The focus of this study is on NDE of battery electrode structures using ultrasonic resonance-based approaches. Ultrasonic resonance data is rich in information regarding the spacing and material properties of the layered structure. Resonance methods are also more sensitive to sub-wavelength features than conventional time-domain approaches. One resonance approach that has been applied to battery inspection is local ultrasonic resonance spectroscopy (LURS). LURS was applied to inspection of lithium metal pouch cells seeded with internal defects by Nelson [3]. Nelson enabled contact-based battery inspections by using a linear system assumption to remove the transducer and delay line effects from the measured resonance response. This work was further advanced by Webster et al., who adapted the contact-based inspection approach to a scanning form-factor first using cells seeded with lithium metal chips [4]. Other notable resonance-based approaches to battery inspection include the work of Huang et al. [5], in which a combination of resonance and time-domain data was

*Corresponding Author: matthew.r.webster@nasa.gov

used to assess changes in the spacing of a multi-layer lithium ion battery during cycling, and work by Liu et al [6] which examined weld-tab quality using the vibration spectra measured with a laser vibrometer.

Prior studies applying ultrasonic resonance-based inspections to battery structures are limited either in the use of single-point inspections [3,5] or in the use of seeded defects that are unrepresentative of real electrode degradation [4]. Here we apply a LURS inspection approach in a scanning form factor in order to examine how resonance changes spatially in various aging scenarios. The work demonstrates the utility of the approach for identifying and characterizing manufacturing defects, and as a means of identifying degradation mechanisms in batteries aged through electrochemical cycling.

2. METHODS

2.1 Specimen Development

Two sets of lithium metal pouch cells were used in this study. Most of the pouch cells examined were single-cells that were fabricated at NASA Glenn Research Center (GRC) in a dry-room using commercial battery components and electrodes (Figure 1a). These components consisted of a nylon/aluminum/polypropylene pouch, lithium metal anodes on a copper current collector, nickel manganese cobalt oxide (NMC) cathodes on an aluminum current collector, Celgard 2325 separators between the anode and cathode layers, and a 1M lithium hexafluorophosphate ($LiPF_6$) in ethylene carbonate : diethyl carbonate : dimethyl carbonate (EC:DEC:DMC, 1:1:1 vol%) electrolyte solution. The resulting capacity for the single cells was approximately 80 mAh.

One multi-cell lithium metal battery was also examined. This battery was produced by Cornerstone Research Group (CRG) and had 12 electrochemical cells in the stack. This multi-layer battery used double-sided lithium metal anodes on copper current collectors and Celgard 2325 separators, with similar cathode materials and electrolyte solution. Note that the exact cathode materials and electrolyte were not disclosed, but also do not affect the analysis below. A total of twelve repeated units consisting of a double-sided anode/current collector, separator, and double-sided cathode/current collector were layered in the battery (Figure 1b). The total nominal capacity was approximately 2 Ah.

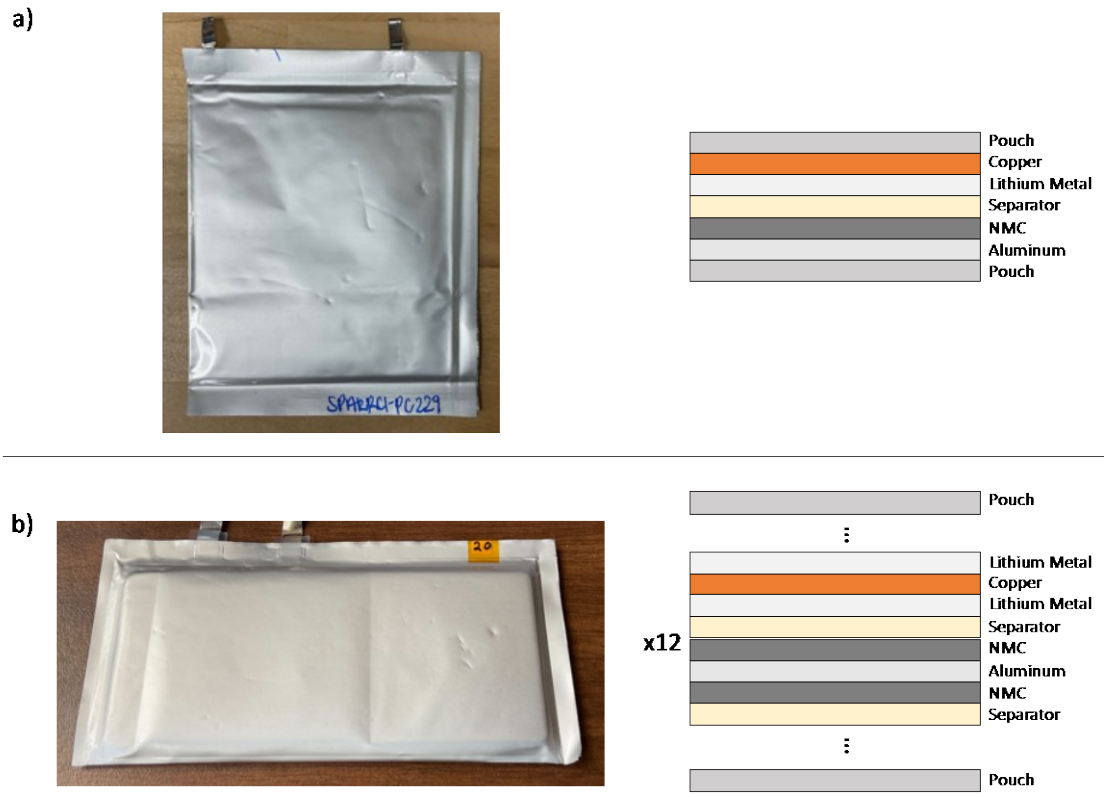

Figure 1: Battery specimens examined during this study. (a) Left – Image of a single lithium metal pouch cell made by NASA GRC. Right – Illustration of the component stacking sequence within the pouch cell. (b) Left – Image of a multi-cell lithium metal battery made by CRG. Right – Illustration of the 12-cell stacking sequence showing the repeated unit of double-sided anode/cathode pairs.

All cells were formed at ambient temperature through constant-current electrochemical cycling at C/20 for 2 cycles and C/10 with a voltage window of 3.0 – 4.25V, where 1C is the charge rate (or C-rate) required to charge the cell in one hour. The cells were then charged to 3.75V at the end of formation at a C-rate of C/10 before cycling at various conditions. While the results presented below do include cells that were unable to maintain a charge, most did undergo electrochemical cycling to seed changes in the as-manufactured electrode structures. Electrochemical cycling was performed under constant-current conditions ranging from C/5 to 2C. Unless otherwise specified, cycling was performed under ambient conditions with uniform pressure applied to the electrode surfaces to consolidate the cells. As noted in the results below, deviations from this standard cycling protocol, including non-uniform electrode loading and low temperature cycling were introduced as well.

2.2 Local Ultrasonic Resonance Spectroscopy

LURS was used to test all of the pouch cells in this study. LURS is an ultrasonic inspection method that evaluates vibrational through-thickness resonances in local region in the plane of the battery. This approach has been employed for fiber reinforced composites in non-contact mode exciting with a pulse laser [7], and in batteries with a pulse-echo ultrasonic transducer configuration [3]. In a pulse-echo configuration, the transducer transmits acoustic energy and then receives reflected energy from the specimen under test. A time delay, such as a fluid path or delay line transducer, allows for the time-domain separation of excited and received waveforms. The received waveforms are then post processed using a linear system deconvolution to identify acoustic resonances in the laterally local, through-thickness region of a component. At resonance frequencies, minima are seen in the frequency spectra of reflected acoustic waves [8] (Figure 2).

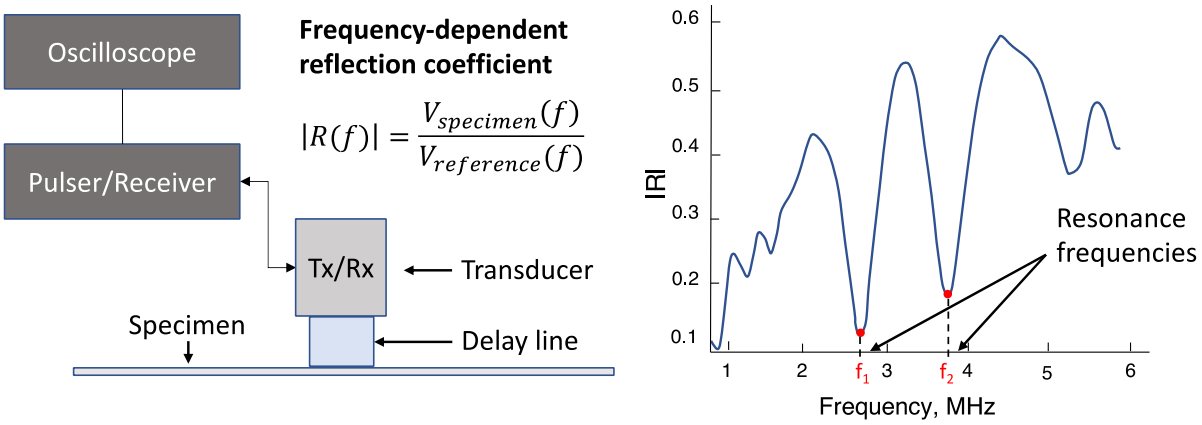

Figure 2: Illustration of the LURS inspection process. Tx/Rx refers to the ultrasonic transducer acting both as a transmitter and receiver in a pulse echo configuration, with an accompanying solid delay line or fluid water path. The amplitude of the frequency-dependent reflection coefficient, |R(f)|, is obtained by a deconvolution of the reflected voltage of the specimen $|V_{Specimen}(f)|$, with the reflected voltage from just the transducer and delay line without the specimen present $|V_{reference}(f)|$, taken in the frequency domain. Resonance frequencies are identified as minima in the resulting reflection spectrum.

Prior studies using the LURS technique on pouch cell battery specimens [3,4] used a transducer in contact with the battery surface to avoid full submersion of the specimen. Nelson [3] showed that influence of the transducer and instrumentation on the reflected frequency spectra can be removed by using a reference measurement, $V_{reference}(f)$, of the transducer response to ultrasonic excitation without the specimen present and then another measurement, $V_{specimen}(f)$, with the specimen present. The theoretical voltage response in both the reference measurement and specimen measurement contain linear transfer functions that alter the initial transducer excitation voltage based on electrical and mechanical interactions with the instrumentation, transducer, and delay line. Due to the linearity of the voltage scaling from the combined transfer functions (which was experimentally verified during test setup) the magnitude of the reflection coefficient can be obtained by deconvolution of the measurement response with the reference response in the frequency domain, that is:

$$|R(f)| = \frac{V_{specimen}(f)}{V_{reference}(f)}. \quad (1)$$

It should be noted that Equation 1 assumes a fixed-length delay line in contact with the battery such that the effect of the delay line (e.g., from attenuation) is constant between reference and specimen measurements. This study, in contrast, used, a flexible "delay line" consisting of a cylindrical column of water contained by a flexible nitrile membrane (Figure 3). The benefit of using this captured water column approach was that it allowed the transducer to be scanned over the specimen without full submersion of the batteries in water. Calibration methods were tailored to this unique situation to enable the reflection spectrum of the battery to be isolated using Equation (1). Specifically, calibration of the captured water column was done using a glass reflector positioned beneath the water column such that the time of flight of the ultrasonic signal from the reflector matched the time of flight received from the front surface of pouch cell specimens during testing.

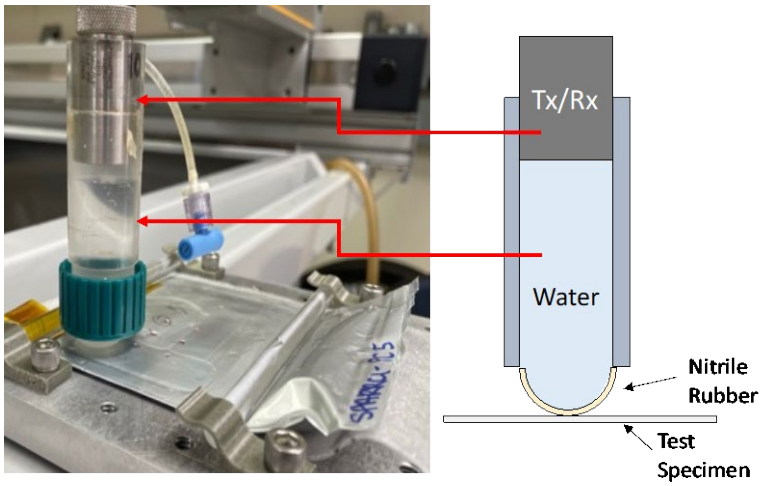

Figure 3: The captured water column used for testing. (Left) Image of the captured water column during LURS measurement of a pouch cell. (Right) Illustration of the captured water column highlighting the different components relative to the test specimen.

Measurements on pouch cell specimens were made using a custom testing fixture with the captured water column connected to a three-axis ultrasonic scanning system (Figure 3). For the single-cell specimens produced by NASA GRC, excess electrolyte in the pouch cells had to be moved outside of the scan region to fully consolidate the electrode structure. This was done using acrylic rods, which were pressed on the scan area and rolled over the surface to squeeze out extra fluid. The acrylic rods were then clipped into place on the boundary of the scan area. This can be seen in the image on the left side of Figure 3.

During measurements, a commercial pulser-receiver was used to excite a 10MHz ultrasonic broadband focused ultrasonic transducer contained within the captured water column. Data was collected at a rate of 180 MS/s using a data acquisition card connected to the scan computer. Scans were conducted over an approximately 3 in x 2 in region with a scanning step size of 0.01 in in the x and y directions. At each pixel location in the scans, a time-domain signal was recorded. The pulse received from the battery specimen in each time-domain signal was centered, zero-padded, and windowed using a Hanning window. A discrete Fourier transform was then used to obtain the frequency spectrum of the pulse. This frequency spectrum was normalized by a reference measurement using Equation 1 to obtain the reflection spectrum at each location.

3. RESULTS

LURS scan results are presented below for five lithium metal pouch cell specimens, which includes four single-layer cells produced by NASA GRC and one multi-cell battery produced by CRG. These selected results represent interesting cases that highlight applications of the LURS inspection approach for examining battery structures.

The first application of the LURS inspection approach was for manufacturing quality control. It was not uncommon for defects to be present in the structure that affected the electrochemical performance, including both the discharge capacity and the internal impedance. It should be noted that many of the manufacturing defects could be seen in conventional amplitude-based scans of the batteries as well, but the LURS inspections produced more data on the size and position of the defects in the electrode region of the cells than was available using amplitude metrics alone.

One example of a manufacturing defect was the presence of FOD. Two cases of this are shown below in Figure 4. On the left side of Figure 4, maps of the root mean squared (RMS) pulse amplitude are shown. These images reveal the location of two different FOD features, which caused a local reduction in the signal amplitude. On the right side of Figure 4, B-scans of the LURS reflection spectrum traced over a line in the scan region (highlighted by a red line on the left plots) are given. The minima in the reflection spectra B-scans, which appear as blue lines in the plots, are where resonance occurs. Of these resonance minima, the lower frequency resonances around 3-4MHz have a particularly clear response to the presence of FOD. For the case of Cell A, the FOD is likely an additional lithium deposit, which increases the thickness of the resonance cavity and leads to a local reduction in the second resonance frequency. For Cell B, however, the FOD is a piece of copper between the copper current collector and pouch. In this case the resonance frequencies increase in the

FOD location, likely because the copper introduces a new reflecting boundary in the cell that has a shallower depth than the resonance cavity between the pouch and the copper current collector of the anode. Note that while we have highlighted changes in the lower resonance frequencies, there are changes at higher resonance frequencies as well. For these specimens these higher frequency resonances have been more variable and less prominent over the inspection region, making them less useful for identifying debris without a more thorough analysis. Even without such analysis, however, the differences in the lower resonance responses in these two cases illustrate the added benefit of resonance data for characterizing the size and type of FOD during manufacturing.

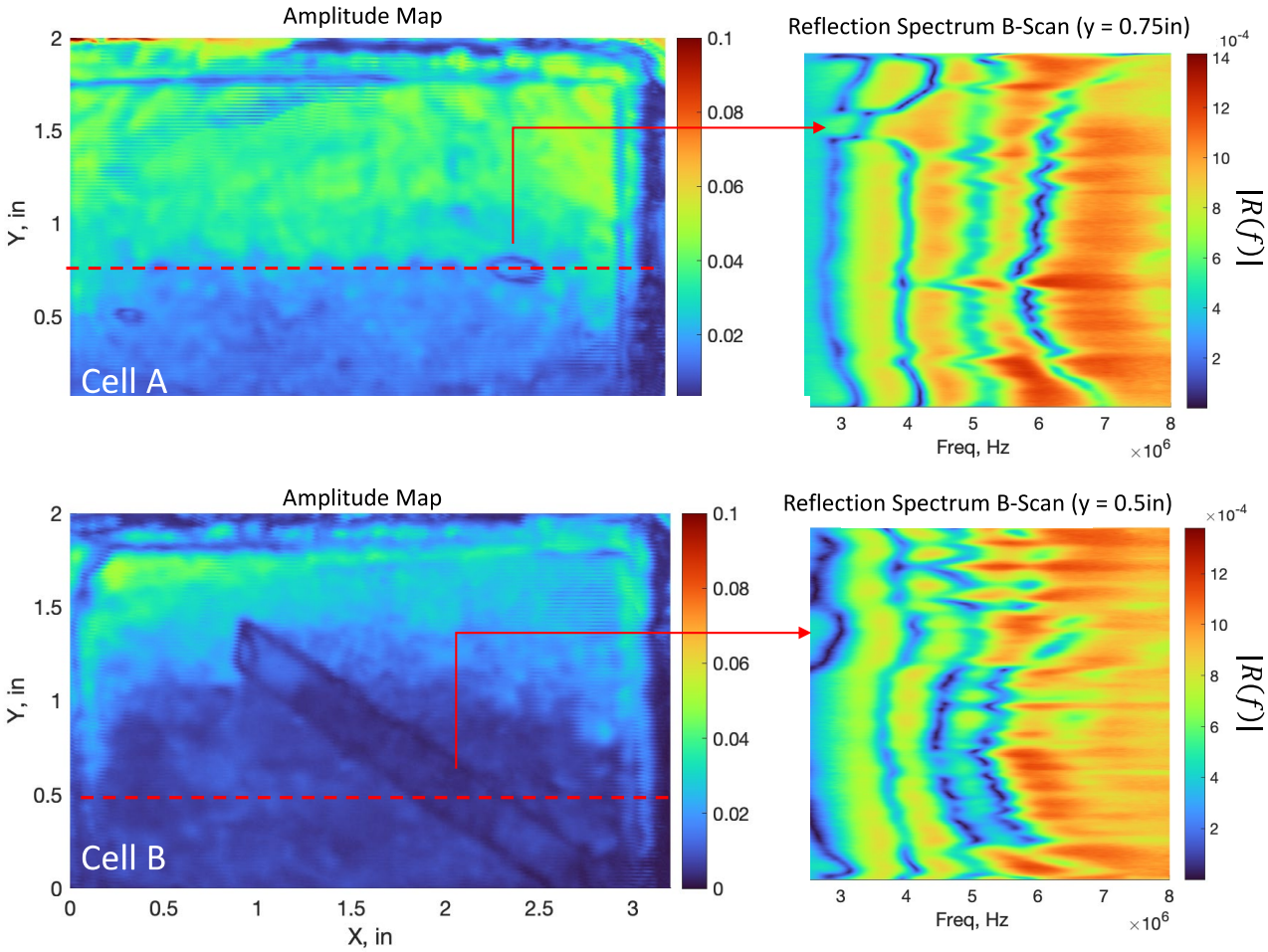

Figure 4: Scan results for two pouch cells produced by NASA GRC with internal FOD defects denoted Cell A and Cell B. (Left) Images of the amplitude of the received pulse at each pixel location. (Right) Line scans (i.e., B-scans) of the reflection spectrum along the horizontal lines indicated in the respective amplitude maps. For both cells, local change in the reflection spectrum is seen at the location of the FOD defect.

Another application of the LURS scanning approach was for examining spatial variation in electrode structure resulting from non-uniform stack pressure during the cycling process. In one such study, a pouch cell was electrochemically cycled at a rate of 2C with only half of the electrode under the compression plate (Figure 5a). The anode structure at end of life was heterogeneous, with areas that built up a significant degradation layer and other areas where the lithium metal layer was bare indicating less activity during cycling (Figure 5b). To highlight the spatial variation in the structure, the reflection spectra measured at each pixel location was analyzed. A peak tracking algorithm was employed to locate the first and second resonance frequency as well as the associated width of the resonance minima (Figure 5c). This data was formed into maps of the resonance frequency distribution over the electrode surface (Figure 5d).

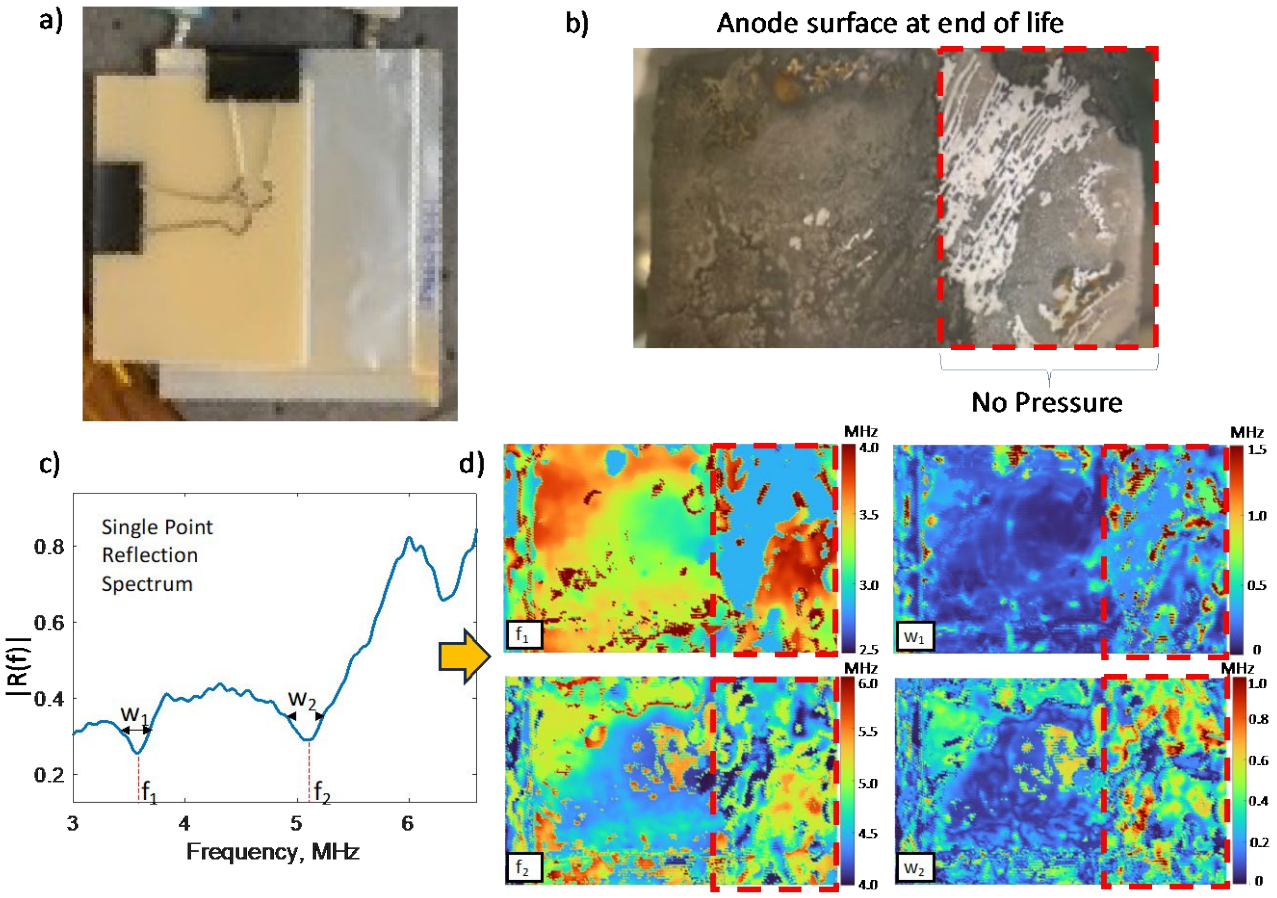

Figure 5: Results from a study on the effects of stack pressure on the electrode surface. (a) Image of the cell during cycling showing pressure plates applied to only half of the cell. The cell was cycled at a rate of 2C. (b) Image of the anode surface after cycling showing a buildup of a dark layer of material on the side of the cell with pressure applied, with the other half showing only intermittent buildup with mostly bare lithium. (c) A representative reflection spectrum measured on the pouch cell which highlights the location of the first and second resonance frequencies (f_1 and f_2) and their respective widths at half prominence (w_1 and w_2). (d) Maps of the resonance features f_1, w_1, f_2, and w_2 over the electrode surface. In these images the region with no pressure applied is highlighted with a dashed red box.

The resonance maps shown in Figure 5d show distinct differences in cell structure between the pressure and no pressure regions. These differences show some correlation with the image anode surface in Figure 5b, but also highlight challenges with scattering in highly irregular regions. For instance, in the maps of both the first and second frequency, lower frequencies are seen in the center of the cell where more uniform deposition is seen on the anode. In the uncompressed region there are higher frequencies where the structure is most uniform. However, in the most irregular areas, peak tracking was challenging because clean resonance minima were not always present.

For cells cycled under constant stack pressure, the LURS approach allows the structural evolution that occurs as lithium is stripped and re-plated on the anode surface to be tracked during the cycling process. Two examples of this are shown below in Figure 6 and Figure 7. The cell in Figure 6 was cycled at a rate of 2C under ambient conditions, while the cell in Figure 7 was cycled at a rate of 0.5C and at a temperature of -20°C. These two cycling conditions led to significant changes in the anode structure at end of life. In the cell cycled in ambient conditions, a degradation layer built up on the anode surface as is typical for lithium metal cells [9] (Figure 6b). Resonance maps produced from LURS scans on this cell show steady reduction in both the first and second resonance frequencies throughout the cycling process as the anode degrades (Figure 6a).

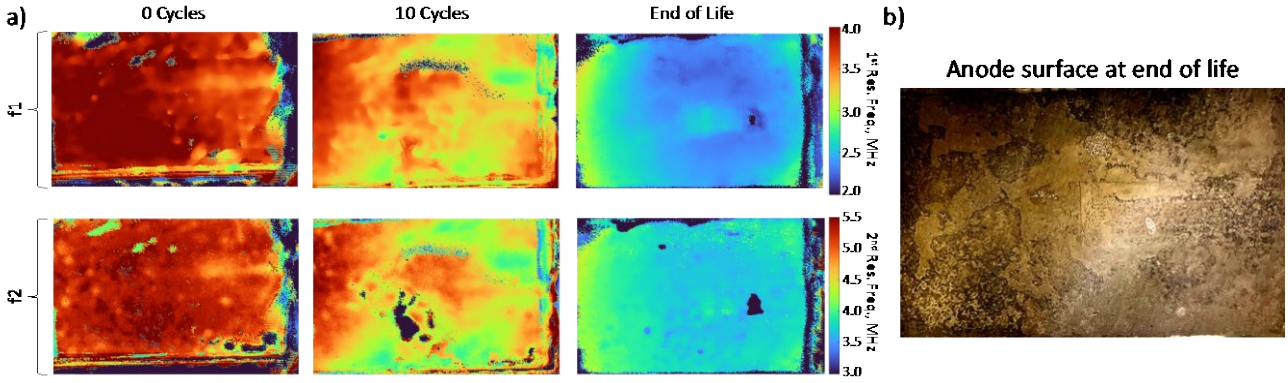

Figure 6: a) Maps of the first and second resonance frequencies (f1 and f2, respectively) for a single cell cycled at 2C under ambient conditions. As the number of cycles is increased, the resonance frequencies move to lower frequencies. b) Photograph of the anode surface at end of life.

The cell cycled under a low temperature condition had much less uniform buildup and degradation on the surface of the anode at end of life. Instead, sporadic mounds of buildup were seen, which are likely electrolyte degradation byproducts and dead lithium on the surface (Figure 7b). The LURS results for this cell show less steady decrease in resonance frequencies compared to the ambient temperature cell, but do show pockets of lower resonance that seem to correspond to some of the locations of buildup seen on the anode. The black regions in Figure 7a, particularly in the plot of the second resonance frequency (f_2) at end of life, are where the peak tracking algorithm failed to find the resonance peak. While this is mainly an artifact resulting from scattering from the mounds of built-up degradation product, it does serve a purpose of identifying scatterers on the surface.

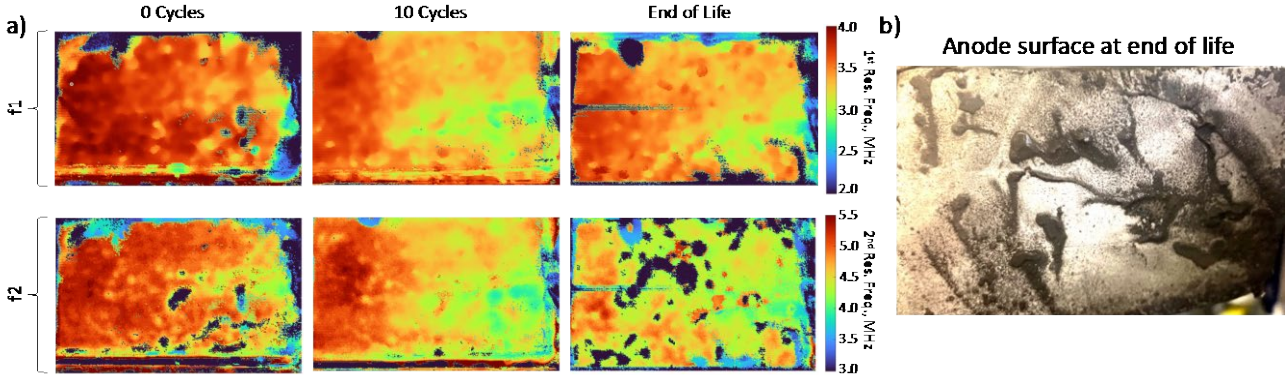

Figure 7: a) Maps of the first and second resonance frequencies (f1 and f2, respectively) for a single cell cycled at 0.5C at a temperature of -20° C. As the number of cycles is increased significantly less change in the average resonance frequency is seen as compared to cells cycled under ambient conditions. b) Photograph of the anode surface at end of life.

In the multi-layer battery, the resonance spectrum was somewhat more challenging to interpret, yet it still provided some insight into the state of the electrodes. In Figure 8, results are given for the 12-cell lithium metal battery after being cycled at a rate of 0.2C to end of life. In Figure 8a resonance frequency and width variation are shown for a resonance minima centered around 9MHz. The data in this case are much noisier than results from single layer cells, likely due to the combined effects of multiple layers on the resonance response at each pixel location. Still, the LURS results highlight a non-uniform buildup on the surface, which is particularly evident in maps of the resonance width. A representative anode surface (front and back) is given in Figure 9b for comparison. It is difficult in this case to correlate the exact patterns of deposition to the resonance frequency or width patterns, since the resonance frequency and width at each pixel location is affected by the structure of each component in the acoustic path. However, from these representative anode images, we see uneven deposition of lithium degradation byproducts that agree qualitatively with the scan results.

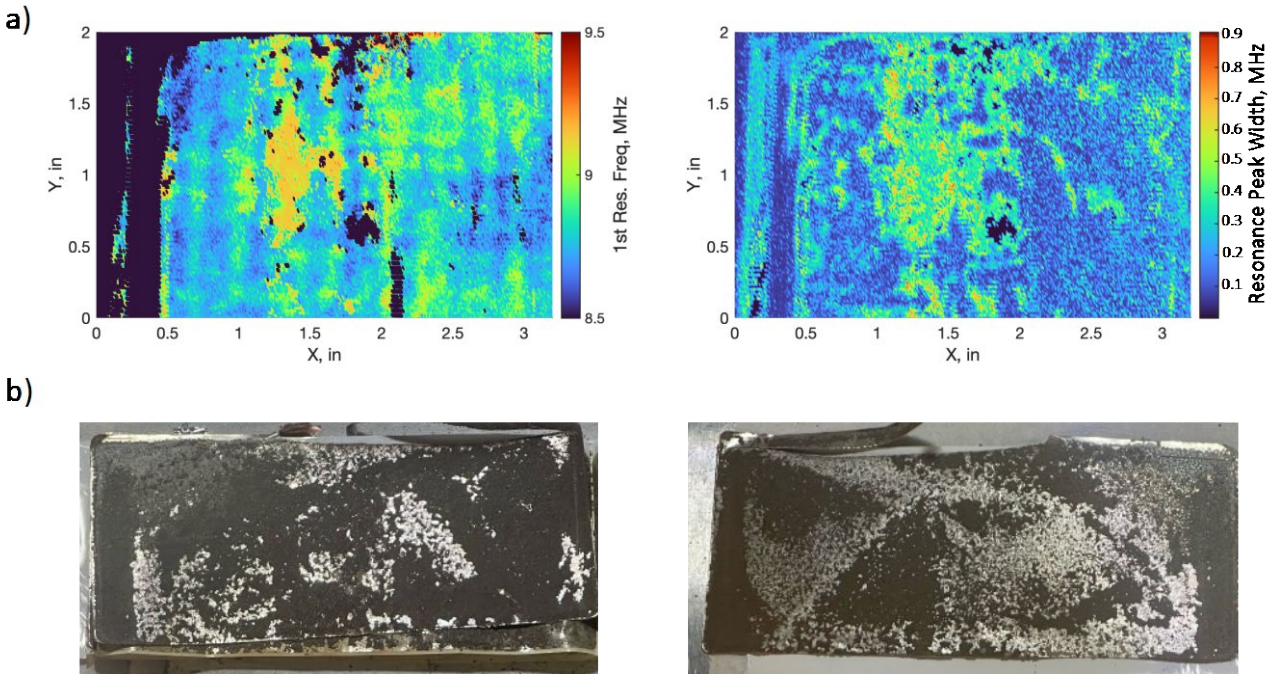

Figure 8: Resonance scan results and images from a cycled 12-layer lithium metal battery at end of life. (a) Resonance results. On the left is a map of the frequency of a resonance peak around 9MHz. On the Right is the width of that peak. Spatial variation is seen across the scan region. (b).

4. DISCUSSION

This study applied a LURS inspection approach to lithium metal pouch cells both in their as-manufactured states and after aging under varying electrochemical and mechanical conditions. The results showed a variety of electrode structures, which were revealed using the LURS resonance spectra. Many of the resonance-based plots that were shown have analogous time- or amplitude-based counterparts, which would be the output from conventional ultrasonic scans. For example, frequency-domain B-scans taken over a line in the inspection area highlighted where changes in the resonance frequency were present in the same way that a conventional B-scan highlights variations in the time of flight. Similarly, resonance maps highlighted the distribution of specific resonance frequencies in the same way that an amplitude or time of flight C-scan map would highlight variation in the attenuation or speed of sound in samples.

Maps of the resonance frequencies appear to be very sensitive to micrometer-scale changes in battery structure. In some cases, maps of the resonance peak widths help to highlight boundaries between different structures as scattering at edges leads to broader resonance peaks that show up as bright regions around features. To take full advantage of the depth of information available from LURS data, development of advanced analytics methods is needed. This includes robust peak-tracking algorithms, image segmentation approaches, and accompanying physics-based models that can be used to determine the underlying cause of a given resonance response. The poroelastic models like those developed by Nelson [3] and Huang [5], for example, could be employed to determine what changes in properties and geometry would lead to a particular pattern of resonance frequencies and widths. The application of these types of models for interpreting scan data was beyond the scope of this study, but will be the focus of future efforts.

ACKNOWLEDGEMENTS

Funding for this work was provided by the NASA Convergent Aeronautics Solutions program “Sensor-based Prognostics to Avoid Runaway Reactions & Catastrophic Ignition (SPARRCI)”. Program management and specimen fabrication was provided by Brianne DeMattia. We thank NASA Office of STEM Engagement (OSTEM) interns Ashley Lam, Daniel

Caicedo, Aoife Zuercher, and Sayyam Deshpande for their contributions in electrochemical testing and physical analysis of battery cells.

REFERENCES

[1] A. D. B. de Lime, T. Lein, S. Maletti, K. Schmal, S. Reuber, C. Heubner and A. Michaelis, "Impact of Electrode Defects on Battery Cell Performance: A Review," *Batteries and Supercaps,* vol. 5, no. 10, 2022.

[2] K.-H. Chen, K. Wood, E. Kazyak, W. LePage, A. Davis, A. Sanchez and N. Dasgupta, "Dead Lithium: Mass transport effects on voltage, capacity, and failure of lithium metal anodes," *Journal of Materials Chemistry A,* no. 23, 2017.

[3] W. Nelson, "Local Ultrasonic Resonance Spectroscopy of Lithium Metal Batteries for Aerospace Applications," *Master's Thesis, University of Virginia,* 2021.

[4] M. Webster, E. Frankforter and P. Juarez, "Evaluation of Ultrasonic Battery Inspection Techniques," *Nondestructive Characterization and Monitoring of Advanced Materials, Aerospace, Civil Infrastructure, and Transportation XVII,* vol. 12487, 2023.

[5] M. Huang, N. Kirkaldy, Y. Zhao, Y. Patel, F. Cegla and B. Lan, "Quantitative Characterization of the Layered Structure Within Lithium-Ion Batteries using Ultrasonic Resonance," *Journal of Energy Storage,* 2022.

[6] H. Liu, S. Laflamme, S. Bentil, R. James, M. McGovern and D. Bruder, "Real-time nondestructive evaluation of electrode weld stacks using a laser vibrometry and shock tube," *Manufacturing Letters,* vol. 37, 2023.

[7] J. Rus and C. Gross, "Local ultrasonic resonance spectroscopy: a demonstration on plate inspection," *Journal of nondestructive evaluation,* 2020.

[8] L. M. Brekhovskikh and O. A. Godin, Acoustics of Layered Media, Berlin: Springer-Verlag, 1989.

[9] Cheng, X. B., Zhang, R., Zhao, C.Z., Wei, F., Zhang, J.G., and Zhang, Q., “A Review of Solid Electrolyte Interphases on Lithium Metal Anode”. *Advanced Science,* Vol. 3, 2015.